Extended x-ray absorption fine structure, x-ray diffraction and reverse Monte Carlo studies of an amorphous $Ga_{50}Se_{50}$ alloy produced by mechanical alloying

2004 J. Phys.: Condens. Matter 16 581

(http://iopscience.iop.org/0953-8984/16/4/007)

INSTITUTE OF PHYSICS PUBLISHING JOURNAL OF PHYSICS: CONDENSED MATTER

J. Phys.: Condens. Matter **16** (2004) 581–590 PII: S0953-8984(04)69495-1

Extended x-ray absorption fine structure, x-ray diffraction and reverse Monte Carlo studies of an amorphous $Ga_{50}Se_{50}$ alloy produced by mechanical alloying

K D Machado[1], P Jóvári[2], J C de Lima[1], C E M Campos[1] and T A Grandi[1]

[1] Departamento de Física, Universidade Federal de Santa Catarina, 88040-900 Florianópolis, SC, Brazil
[2] Hamburger Synchrotronstrahlungslabor HASYLAB am Deutschen Elektronen-Synchrotron DESY, Notkestrasse, 85, D-22603, Hamburg, Germany

E-mail: kleber@fisica.ufsc.br (K D Machado)

Received 24 September 2003, in final form 9 December 2003
Published 16 January 2004
Online at stacks.iop.org/JPhysCM/16/581 (DOI: 10.1088/0953-8984/16/4/007)

Abstract

The local atomic order of an amorphous $Ga_{50}Se_{50}$ alloy produced by mechanical alloying (MA) was studied by the extended x-ray absorption fine structure (EXAFS) and x-ray diffraction (XRD) techniques and by reverse Monte Carlo (RMC) simulations of its total x-ray structure factor. The coordination numbers and interatomic distances for the first neighbours were determined by means of EXAFS analysis and RMC simulations. The RMC simulations also furnished the partial pair distribution functions $G^{\mathrm{RMC}}_{\mathrm{Ga-Ga}}(r)$, $G^{\mathrm{RMC}}_{\mathrm{Ga-Se}}(r)$ and $G^{\mathrm{RMC}}_{\mathrm{Se-Se}}(r)$. The results obtained indicated that there are important differences among the local structure of the amorphous $Ga_{50}Se_{50}$ alloy produced by MA and those of the corresponding crystals, since there are Se–Se pairs in the first coordination shell of the amorphous alloy that are forbidden in the $Ga_{50}Se_{50}$ crystals.

(Some figures in this article are in colour only in the electronic version)

1. Introduction

In the recent years there has been an increase in the number of applications related to nonlinear optical materials. However, the desired properties concerning such applications, such as optical homogeneity, laser damage threshold, stability of the compound upon exposure to laser beam, ease of fabrication, improved mechanical strength and the possibility of making large crystals, are difficult to find in a single material. Gallium selenide (GaSe) has a number of interesting properties for electrical and nonlinear optics applications [1–3]. Crystalline

GaSe is a semiconductor of the III–VI family like GaS and InSe and it has a layered graphite type structure with a fourfold layer, in the sequence Se–Ga–Ga–Se. The crystal cleaves very easily along the layers [1]. At room temperature, the layers are bound by weak van der Waals-type interactions. The weakness of this interaction explains the existence of a number of polytypes [4]. $Ga_{50}Se_{50}$ alloys can be prepared by the melting, vapour deposition and molecular beam epitaxy techniques [5–8]. These techniques have had very limited success because they do not have control over the kinetics and morphology. In addition, due to the low melting points of the elemental Ga (30 °C) and Se (217 °C) and the high vapour pressure of Se above 600 °C it is difficult to obtain Ga–Se alloys at specific compositions. On the other hand, the mechanical alloying (MA) technique [9] can be used to overcome these difficulties since the temperatures reached in MA are very low, which reduces reaction kinetics, allowing the production of poorly crystallized or amorphous materials [10–13] even if the constituents of the alloy have low melting points, as in the case of gallium and selenium. In a recent paper [14] the formation of an amorphous $Ga_{50}Se_{50}$ alloy (a-$Ga_{50}Se_{50}$) by MA was studied as a function of the milling time by using x-ray diffraction (XRD), differential scanning calorimetry (DSC) and Raman scattering (RS) techniques. The results indicated that after 3 h of milling a crystalline alloy was formed. A crystalline-to-amorphous transition occurs with the sample and after 10 h of milling no further structural changes could be detected with x-ray diffraction. Some features of the RS data measured after 10 and 15 h of milling are interesting; for instance there is a Raman band at 235 cm^{-1}, which is usually associated with A_1 and E modes of Se chains [15–19], but the DSC measurement does not indicate amorphous (a-Se) or crystalline (c-Se) selenium. Since our previous study of $Ge_{30}Se_{70}$ alloy [20] indicated that it has an unexpectedly high quantity of Se–Se pairs in the first coordination shell, we were interested in studying the local atomic structure of a-$Ga_{50}Se_{50}$ to determine coordination numbers, interatomic distances and bond angle distributions and to verify whether this alloy also has Se–Se pairs in the first coordination shell, since its crystalline counterparts do not allow this possibility. In order to accomplish this study, we made extended x-ray absorption fine structure (EXAFS) and XRD measurements on it, and its XRD pattern was simulated by using the reverse Monte Carlo simulation (RMC) technique [21–24]. From the simulations we obtained the partial pair distribution functions $G^{\mathrm{RMC}}_{\mathrm{Ga-Ga}}(r)$, $G^{\mathrm{RMC}}_{\mathrm{Ga-Se}}(r)$ and $G^{\mathrm{RMC}}_{\mathrm{Se-Se}}$ which allow us to calculate the desired quantities.

2. Theoretical background

2.1. Structure factors

2.1.1. Faber and Ziman structure factors. According to Faber and Ziman [25], the total structure factor $\mathcal{S}(K)$ is obtained from the scattered intensity per atom $I_{\mathrm{a}}(K)$ through

$$\mathcal{S}(K) = \frac{I_{\mathrm{a}}(K) - [\langle f^2(K)\rangle - \langle f(K)\rangle^2]}{\langle f(K)\rangle^2} = \sum_{i=1}^{n}\sum_{j=1}^{n} w_{ij}(K)\mathcal{S}_{ij}(K), \tag{1}$$

where K is the transferred momentum, $\mathcal{S}_{ij}(K)$ are the partial structure factors and $w_{ij}(K)$ are given by

$$w_{ij}(K) = \frac{c_i c_j f_i(K) f_j(K)}{\langle f(K)\rangle^2}, \tag{2}$$

and

$$\langle f^2(K)\rangle = \sum_i c_i f_i^2(K),$$

$$\langle f(K)\rangle^2 = \left[\sum_i c_i f_i(K)\right]^2.$$

Here, $f_i(K)$ is the atomic scattering factor and c_i is the concentration of atoms of type i. The partial reduced distribution functions $G_{ij}(r)$ are related to $\mathcal{S}_{ij}(K)$ through

$$G_{ij}(r) = \frac{2}{\pi}\int_0^\infty K[\mathcal{S}_{ij}(K) - 1]\sin(Kr)\,\mathrm{d}K. \tag{3}$$

From the $G_{ij}(r)$ functions the partial radial distribution function $\mathrm{RDF}_{ij}(r)$ can be calculated using

$$\mathrm{RDF}_{ij}(r) = 4\pi\rho_0 c_j r^2 + rG_{ij}(r). \tag{4}$$

where ρ_0 is the density of the alloy (in atoms Å^{-3}). Interatomic distances are obtained from the maxima of $G_{ij}(r)$ and coordination numbers are calculated by integrating the peaks of $\mathrm{RDF}_{ij}(r)$.

2.2. RMC method

The basic idea and the algorithm of the standard RMC method are described elsewhere [21–24] and its application to different materials is reported in the literature [10, 20, 26–39]. In the RMC procedure, a three-dimensional arrangement of atoms with the same density and chemical composition of the alloy is placed into a cell (usually cubic) with periodic boundary conditions and the $G_{ij}^{\mathrm{RMC}}(r)$ functions corresponding to it are directly calculated through

$$G_{ij}^{\mathrm{RMC}}(r) = \frac{n_{ij}^{\mathrm{RMC}}(r)}{4\pi\rho_0 r^2\Delta r}, \tag{5}$$

where $n_{ij}^{\mathrm{RMC}}(r)$ is the number of atoms at a distance between r and $r + \Delta r$ from the central atom, averaged over all atoms. By allowing the atoms to move (one at a time) inside the cell, the $G_{ij}^{\mathrm{RMC}}(r)$ functions can be changed and, as a consequence, $\mathcal{S}_{ij}^{\mathrm{RMC}}(K)$ and $\mathcal{S}^{\mathrm{RMC}}(K)$ are changed. Thus, $\mathcal{S}^{\mathrm{RMC}}(K)$ is compared to the $\mathcal{S}(K)$ factor in order to minimize the differences between them. The function to be minimized is

$$\psi^2 = \frac{1}{\delta}\sum_{i=1}^{m}[\mathcal{S}(K_i) - \mathcal{S}^{\mathrm{RMC}}(K_i)]^2, \tag{6}$$

where the sum is over m experimental points and δ is related to the experimental error in $\mathcal{S}(K)$. If the movement decreases ψ^2, it is always accepted. If it increases ψ^2, it is accepted with a probability given by $\exp(-\Delta\psi^2/2)$; otherwise it is rejected. As this process is iterated ψ^2 decreases until it reaches an equilibrium value. Thus, the atomic configuration corresponding to equilibrium should be consistent with the experimental total structure factor within the experimental error. By using the $G_{ij}^{\mathrm{RMC}}(r)$ functions the coordination numbers and interatomic distances can be calculated. In addition, the bond angle distributions $\Theta_{ijl}(\cos\theta)$ can also be determined.

3. Experimental procedures

a-$Ga_{50}Se_{50}$ was produced by considering a binary mixture of high purity elemental powder of selenium (Alfa Aesar 99.999% purity, particle size <150 μm) and scraped ingots of gallium (Aldrich, 99.999% purity) that was sealed together with several steel balls (with diameter of about 1 mm) into a cylindrical steel vial under an argon atmosphere. The ball-to-powder weight ratio was 10:1. A high energy ball mill Spex Mixer/Mill model 8000 (working at 1200 rpm)

was used to perform MA at room temperature. A ventilation system was used to keep the vial temperature close to room temperature. The sample was milled for 15 h and analysed by energy dispersive spectroscopy (EDS) measurements in a scanning electron microscope and Mössbauer spectroscopy in order to determine possible contamination by the milling media. The EDS results were: 49 at.% Se and 51 at.% Ga. There was no evidence of bulk Fe or Fe compounds in the Mössbauer spectrum. The samples were formed by placing the powder onto a porous membrane (Millipore, 0.2 μm pore size) in order to achieve optimal thickness (about 50 μm), and neither Kapton tape nor BN were used. The EXAFS measurements were carried out at room temperature in the transmission mode on the D04B beamline of LNLS (Campinas, Brazil), using a channel cut monochromator (Si 111) and two ionization chambers filled with air as detectors, working at 10% and 70% efficiency, respectively, and the beam size at the sample was about 1×3 mm^2. This yielded a resolution of about 3.0 eV on Ga and Se K edges. At these energies, harmonic rejection is irrelevant at the D04B beamline. The energy and average current of the storage ring were 1.37 GeV and 120 mA, respectively.

The XRD measurements were carried out at the BW5 beamline [40] at HASYLAB. All data were taken at room temperature using a Si(111) monochromator and a Ge solid state detector. The energy of the incident beam was 121.3 keV ($\lambda = 0.102$ Å). The cross section of the beam was 1×4 mm^2 ($h \times v$). Powder sample was filled into a thin walled (10 μm) quartz capillary with 2 mm diameter. The energy and average current of the storage ring were 4.4 GeV and 110 mA, respectively. To check for possible instabilities of the beam and the detector electronics, scattered intensities were recorded in ten subsequent scans. Raw intensity was corrected for dead time, background, polarization, detector solid angle and Compton scattering as described in [40]. The total structure factor was computed from the normalized intensity $I_a(K)$ according to Faber and Ziman [25] (see equation (1)).

4. Results and discussion

4.1. EXAFS measurements

The unfiltered EXAFS oscillations $\chi(k)$ at both K edges are shown in figure 1 and the absolute value of their Fourier transforms ($k^3\chi(k)$ on the Ga edge, 3.8–14.3 Å^{-1}, and $k\chi(k)$ on the Se edge, 3.4–14.3 Å^{-1}, both using a Hanning weighting function), after standard data reduction procedures using Winxas97 software [41], are seen in figure 2. Since they are of high quality the EXAFS oscillations shown in figure 1 were directly fitted by using Gaussian distributions to represent the homopolar and heteropolar bonds [42]. We also used the third cumulant option of Winxas97 to investigate the presence of asymmetric shells. The amplitude and phase shifts relative to the homopolar and heteropolar bonds needed to fit them were obtained from *ab initio* calculations using the spherical waves method [43] and by the FEFF software. The fitting results on Ga and Se edges are also shown in figure 1.

Structural parameters extracted from the fits are listed in table 1. Two things are worth mentioning at this point: first, the upper limit of the first coordination shell is very well defined and the contribution of more distant shells is negligible; second, the very good fits shown in figure 1 were achieved only when Se–Se pairs were considered in the first shell. This fact indicates that the local structure of a-$Ga_{50}Se_{50}$ produced by MA is different from its crystalline counterparts as none of the known stable crystalline $Ga_{50}Se_{50}$ structures contains Se–Se bonds, and it can explain the Raman band at 235 cm^{-1} observed in the RS data of this alloy, which can be seen in figure 3 of [14]. The high quantity of Se–Se pairs determined by EXAFS and the Raman band associated with Se_n chains could indicate the presence of c-Se or a-Se in the alloy, but its DSC measurement (figure 2 of [14]) does not show the melting of c-Se, which

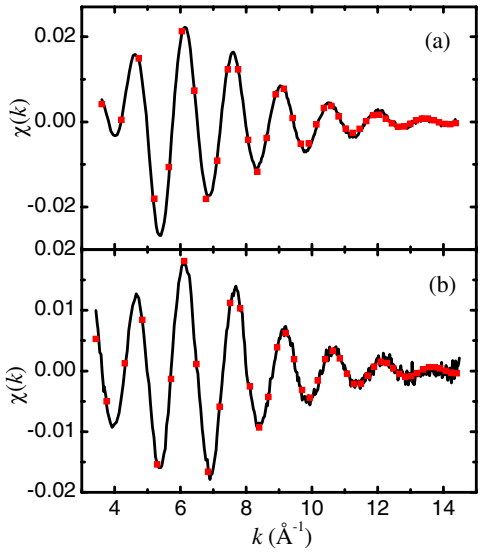

Figure 1. Experimental EXAFS spectra (full curve) and their simulations (squares) for a-$Ga_{50}Se_{50}$ on the (a) Ga K edge, (b) Se K edge.

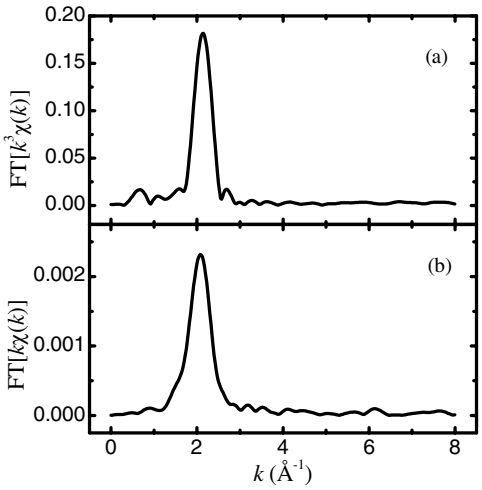

Figure 2. Fourier transformation of experimental EXAFS spectra: (a) on the Ga K edge and (b) on the Se K edge.

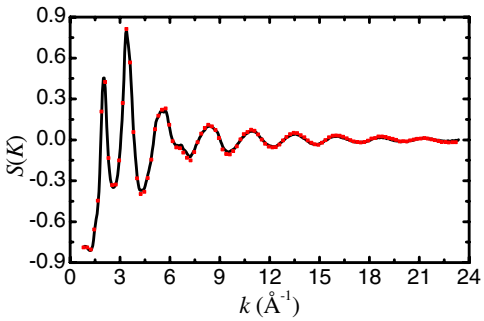

Figure 3. Experimental (full curve) and simulated (squares) total structure factors for a-$Ga_{50}Se_{50}$.

should appear around 217 °C, nor the glass transition or crystallization of a-Se, which should occur at about 45 and 90 °C, respectively [44, 45]. Concerning these features, the structure of our a-$Ga_{50}Se_{50}$ alloy is different from that found in liquid $Ga_{50}Se_{50}$ (l-$Ga_{50}Se_{50}$) studied by neutron diffraction (ND) [46] and by molecular dynamics simulations (MD) [47, 48], which could be attributed to the preparation method since samples produced by MA contain many more structural defects and vacancies than those produced by melting. It is to be mentioned that Se–Se bonding can also be found in Ge_xSe_{1-x} and $Ge_xSe_yZn_z$ thin films produced by rf sputtering as was reported in a recent EXAFS study [49].

4.2. X-ray diffraction and RMC simulations

Figure 3 shows the experimental XRD $\mathcal{S}(K)$ (full curve). It resembles the ND $\mathcal{S}(K)$ shown in [46] or [47] for l-$Ga_{50}Se_{50}$ but it has some important differences. The two first peaks for our

Table 1. Structural parameters obtained for a-$Ga_{50}Se_{50}$. The numbers in parentheses are the errors.

EXAFS				
	Ga K edge		Se K edge	
Bond type	Ga–Ga	Ga–Se	Se–Ga	Se–Se
N	1.6(0.5)	2.4(0.4)	2.4(0.4)	1.5(0.4)
r (Å)	2.39(0.02)	2.46(0.02)	2.46(0.02)	2.40(0.02)
σ^2 (Å $\times 10^{-2}$)	1.26	0.623	0.623	1.78
RMC				
Bond type	Ga–Ga	Ga–Se	Se–Ga	Se–Se
N	1.2	2.5	2.5	1.3
r (Å)	2.42	2.42	2.42	2.42
$Ga_{50}Se_{50}$ compound[a]				
Bond type	Ga–Ga	Ga–Se	Se–Ga	Se–Se
N	1	3	3	6
r (Å)	2.44	2.45	2.45	3.75
$Ga_{50}Se_{50}$ compound[b]				
Bond type	Ga–Ga	Ga–Se	Se–Ga	Se–Se
N	1	3	3	6[c]
r (Å)	2.39	2.47	2.47	3.74

[a] Space group $P6_3/mmc$.
[b] Space group $P\bar{6}m2$.
[c] The trigonal crystal of space group $R3m$ has four Se–Se pairs.

alloy are narrower and better defined, the second peak is located at 3.3 $Å^{-1}$ in a-$Ga_{50}Se_{50}$ and it is found at 3.0 $Å^{-1}$ for l-$Ga_{50}Se_{50}$ and the third peak, at 5.7 $Å^{-1}$, has a shoulder at 6.7 $Å^{-1}$ that is not seen for l-$Ga_{50}Se_{50}$. These features at medium K indicate that the local structure of a-$Ga_{50}Se_{50}$ is really different from that found in l–a-$Ga_{50}Se_{50}$, as the EXAFS analysis and RS data had indicated.

$\mathcal{S}(K)$ was modelled by reverse Monte Carlo simulations [21–24] using cubic cells with 1600 and 12 800 atoms. The average density was $\rho_0 = 0.039\,07$ atoms $Å^{-3}$. This value was found from the slope of the straight line $(-4\pi\rho_0 r)$ fitting the initial part (up to the first minimum) of the total $G(r)$ function [50]. The minimum distance of atoms was also extracted from $G(r)$ and fixed at 2.18 Å. All the simulations were performed considering atoms randomly placed in the cubic cells as starting configurations. Then the following series of simulations were carried out:

(i) Hard sphere simulation without experimental data to avoid possible memory effects of the initial configurations in the results.

(ii) '*Unconstrained' runs* (i.e. when experimental data were 'switched on'). These runs led to three essentially identical partial pair correlation functions and partial structure factors which can be considered as linear combinations of the 'true' partial quantities. It is to be mentioned that as neither the size nor other *a priori* information can distinguish between Ga and Se atoms at this step no adequate coordination numbers can be obtained.

(iii) '*Constrained' runs*. The experimental $\mathcal{S}(K)$ was fitted by using EXAFS coordination number values as initial guesses, which were then allowed to vary around the starting

values. Comparison of experimental (full curve) and calculated (squares) structure factors for the latter case is shown in figure 3, the partial pair correlation functions are given in figure 4 and structural parameters obtained from the simulation are found in table 1. EXAFS and RMC results show a very good agreement with each other, mainly, if we consider that EXAFS data have an error of about 0.5 atoms in the partial coordination numbers and 0.02 Å in the interatomic distances for such alloys. As has already been pointed out EXAFS signals at both edges contain almost exclusively contributions of the first coordination shells. Therefore we believe that using the coordination numbers derived from EXAFS instead of fitting diffraction and EXAFS data simultaneously is justifiable as we can incorporate all the element specific information obtained by EXAFS in our simulation model in a simple and computationally cheap way.

(iv) The whole series of calculations was repeated from the very beginning with the difference that during the 'constrained' run random steps resulting in non-zero Se–Se first coordination number were rejected. It is important to note that if Se–Se pairs were forbidden as first neighbours the simulations did not converge, reinforcing the results obtained by EXAFS analysis.

The $G_{ij}^{\mathrm{RMC}}(r)$ functions can be seen in figure 4. There are important differences between these functions and those found for l-$Ga_{50}Se_{50}$ using MD [47, 48]. We should note some points here:

(a) Both ND [46] and MD [47, 48] studies were performed on l-$Ga_{50}Se_{50}$ at 1030 and 1027 °C, respectively, and there are many systems where the local environment changes upon melting (for example water and Si).

(b) RMC is a rather unsophisticated tool as it works with a minimum amount of *a priori* information (density, hard sphere diameter); therefore the deterioration of the quality of the fit after introducing additional constraints suggests that these constraints are non-physical, and this happens with our simulations if we try to force the coordination numbers obtained by MD simulations.

(c) We tried to fit EXAFS data using MD results and only unreasonable fits were found. On the basis of these points, we believe our $G_{ij}^{\mathrm{RMC}}(r)$ functions should really not be the same as those found by MD simulations.

$G_{\mathrm{Ga-Ga}}^{\mathrm{MD}}(r)$ in l-$Ga_{50}Se_{50}$ has two not well-isolated peaks at 2.51 and 3.75 Å and a slight indication of a third peak at about 5.5 Å, whereas the two first peaks of our $G_{\mathrm{Ga-Ga}}^{\mathrm{RMC}}(r)$ function are well defined and located at 2.42 and 3.87 Å, and the third peak is clearly seen at 5.82 Å. The three first peaks of $G_{\mathrm{Ga-Se}}^{\mathrm{RMC}}(r)$ are seen at 2.42, 3.89 and 5.89 Å, and these positions are close to those found for c-GaSe. On the other hand, the MD results on l-$Ga_{50}Se_{50}$ show only very small indications of peaks beyond 3 Å. The first peak of $G_{\mathrm{Se-Se}}^{\mathrm{RMC}}(r)$ occurs at 2.42 Å, indicating that there are Se–Se pairs in a-$Ga_{50}Se_{50}$ in the first coordination shell, in agreement with EXAFS results. The next two peaks are found at 4.0 and 5.95 Å, which are relatively close to Se–Se peak positions in c-GaSe. Both c-GaSe and l-$Ga_{50}Se_{50}$ do not have Se–Se pairs as first neighbours, and this is the most important difference between these alloys and ours. We should note that in l-$Ga_{50}Se_{50}$ the $G_{\mathrm{Se-Se}}(r)$ function obtained by MD shows a weak indication of a Se–Se coordination shell at 2.45 Å (see figure 6 of [47] or figure 3 of [48]), which becomes clearer for l-Ga_2Se_3. This suggests that even in the liquid state Se–Se pairs show a tendency to be formed, which is enhanced in the amorphous alloy produced by MA.

The positions of the first and second peaks in all of the $G_{ij}^{\mathrm{RMC}}(r)$ correspond to a mean bond angle of 107° for the four bond types (Ga–Ga–Ga, Se–Se–Se, Ga–Se–Se, Ga–Ga–Se) that can be directly derived from the $G_{ij}^{\mathrm{RMC}}(r)$ peak positions. As this is very close to the value

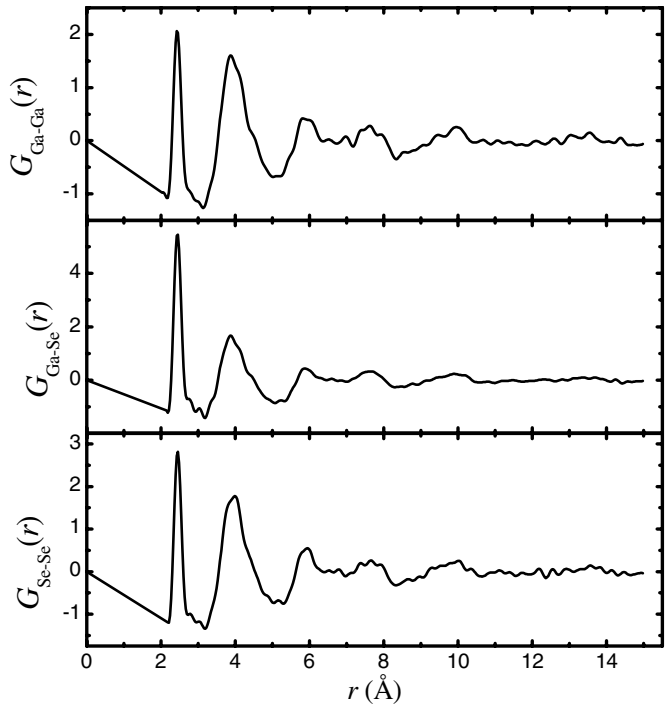

Figure 4. $G^{\text{RMC}}_{\text{Ga-Ga}}(r)$, $G^{\text{RMC}}_{\text{Ga-Se}}(r)$ and $G^{\text{RMC}}_{\text{Se-Se}}(r)$ functions obtained from the RMC simulations.

describing perfect tetrahedral coordination (109.5°) and $N_{\text{GaGa}} + N_{\text{GaSe}}$ and $N_{\text{SeSe}} + N_{\text{SeGa}}$ are both close to 4 it is evident that we can assume that a-$Ga_{50}Se_{50}$ produced by MA has a tetrahedral structure with a definite tendency to form homopolar bonds.

As a cross-check we compared our diffraction data with the structure factor of a-Si, a tetrahedrally coordinated system [51]. To account for the differences of bond lengths and densities (2.36 Å and 0.0505 Å^{-3} for a-Si, respectively) both K-values and amplitudes of a-Si $\mathcal{S}(K)$ were scaled down with the ratio of the corresponding values (0.975 and 0.774, respectively) and they can be seen in figure 5. In our opinion the good agreement between the two data sets is a very convincing illustration that the local structure of a-$Ga_{50}Se_{50}$ is also tetrahedral.

The difference of the Ga–Ga and Ga–Se bond lengths in the crystalline modifications is not greater than about 0.08 Å (see table 1) and they are also quite close to the value of 2.35 Å found recently for a-Se [29]. As the spatial resolution of diffraction experiments is equal to π/K_{max} the $\mathcal{S}(K)$ factor should be measured at least up to 40 Å^{-1} to get more detailed information on the first coordination shell. It should also be mentioned that due to the value of the neutron scattering lengths ($b_{\text{Se}} = 7.970$ fm, $b_{\text{Ga}} = 7.288$ fm) neutron diffraction data would give essentially the same information. Other techniques used to obtain information at the level of $G_{ij}(r)$ are either prohibitively expensive (neutron diffraction with isotopic substitution) or yield limited spatial resolution due to the low K_{max} value available (anomalous x-ray scattering).

5. Conclusion

In summary the local structure of an amorphous $Ga_{50}Se_{50}$ alloy produced by MA was investigated experimentally with EXAFS and high energy x-ray diffraction. EXAFS analysis

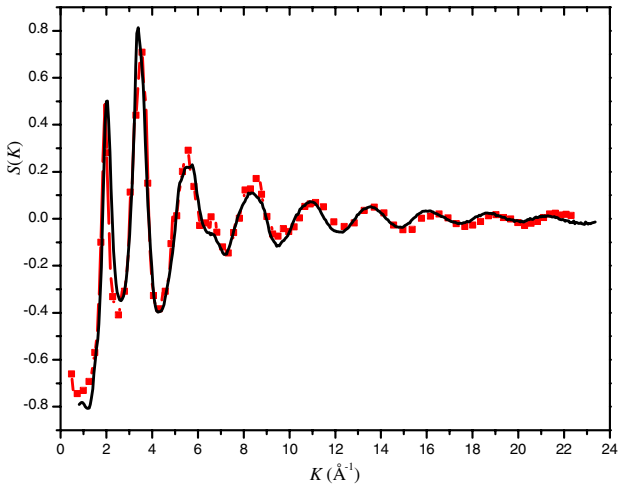

Figure 5. Comparison between rescaled a-Si (squares) and a-$Ga_{50}Se_{50}$ (full line) $\mathcal{S}(K)$ factors.

led to the following conclusions: the average first coordination number in a-$Ga_{50}Se_{50}$ is close to 4, indicating a tetrahedral local structure, Ga and Se local environments are similar and Se–Se bonding is significant. This last conclusion is confirmed by the RS and DSC data seen in [14]. All of these findings were checked and confirmed by RMC study of diffraction data: it was possible to obtain a good fit with coordination constraints close to the EXAFS values while runs without Se–Se first neighbours led to a poor agreement between model and experiment.

The present study illustrates how complementary information obtained by different experimental techniques can be combined within the framework of reverse Monte Carlo simulation. We believe that this is a useful and efficient way of modelling disordered materials especially in cases where traditional methods (e.g. neutron diffraction with isotopic substitution) are not appropriate.

Acknowledgments

The Brazilian authors wish to thank the Brazilian agencies CNPq and CAPES for financial support. This study was also partially supported by LNLS (Proposal No XAS 998/01). P Jóvári is indebted to Hermann Franz and Martin von Zimmermann (both of HASYLAB) for their help during the diffraction measurement and to L Pusztai (RISSPO, Budapest) for sending the data on a-Si.

References

[1] Fernelius N C 1994 *Prog. Cryst. Growth Charact.* **28** 275
[2] Singh N B, Suhre D R, Rosch W, Meyer R, Marable M, Fernelius N C, Hopkins F K, Zelmon D E and Narayanan R 1999 *J. Cryst. Growth* **198/199** 588
[3] Singh N B, Suhre D R, Balakrishna V, Marable M, Meyer R, Fernelius N C, Hopkins F K and Zelmon D E 1998 *Prog. Cryst. Growth Charact.* **37** 47
[4] Jandl S, Brebner J L and Powell B M 1976 *Phys. Rev.* B **13** 686
[5] Ludviksson A, Rumaner L E, Rogers J W J and Ohuchi F S 1995 *J. Cryst. Growth* **151** 114
[6] Fujita K, Izumi T, Ohsaki K, Tambo T, Ueba H and Tatsuyama C 1994 *Thin Solid Films* **247** 134
[7] Stoll S L, Gillan E G and Barron A R 1996 *Adv. Mater.* **8** 182

[8] Ng T L, Maung N, Fan G, Poole I B, Williams J O, Wright A C, Foster D F and Cole-Hamilton D J 1996 *Chem. Vapor Depos.* **2** 185
[9] Suryanarayana C 2001 *Prog. Mater. Sci.* **46** 1
[10] Machado K D, de Lima J C, de Campos C E M, Grandi T A and Trichês D M 2002 *Phys. Rev.* B **66** 094205
[11] Campos C E M, de Lima J C, Grandi T A, Machado K D and Pizani P S 2002 *Solid State Commun.* **123** 179
[12] Campos C E M, de Lima J C, Grandi T A, Machado K D and Pizani P S 2002 *Physica* B **324** 409
[13] de Lima J C, dos Santos V H F and Grandi T A 1999 *Nanostruct. Mater.* **11** 51
[14] Campos C E M, de Lima J C, Grandi T A, Machado K D and Pizani P S 2003 *Solid State Commun.* **126** 611
[15] Wang Y, Matsuda O, Inoue K, Yamamuro O, Matsuo T and Murase K 1998 *J. Non-Cryst. Solids* **232–234** 702
[16] Popovic Z V, Jakšić Z, Raptis Y S and Anastassakis E 1998 *Phys. Rev.* B **57** 3418
[17] Takeuchi H, Matsuda O and Murase K 1998 *J. Non-Cryst. Solids* **238** 91
[18] Gulbrandsen E, Johnsen H B, Endregaard M, Grande T and Stølen S 1999 *J. Solid State Chem.* **145** 253
[19] Kohara S, Goldbach A, Koura N, Saboungi M-L and Curtiss L A 1998 *Chem. Phys. Lett.* **287** 282
[20] Machado K D, de Lima J C, Campos C E M, Grandi T A and Pizani P S 2004 *J. Chem. Phys.* at press
[21] McGreevy R L and Pusztai L 1988 *Mol. Simul.* **1** 359
[22] McGreevy R L 1995 *Nucl. Instrum. Methods Phys. Res.* A **354** 1
[23] McGreevy R L, Howe M A and Wicks J D 1993 RMCA version 3, available at http://www.studsvik.uu.se
[24] McGreevy R L 2001 *J. Phys.: Condens. Matter* **13** 877
[25] Faber T E and Ziman J M 1965 *Phil. Mag.* **11** 153
[26] Rosi-Schwartz B and Mitchell G R 1994 *Polymer* **35** 5398
[27] Mellergard A and McGreevy R L 1999 *Acta Crystallogr.* A **55** 783
[28] Karlsson L, Wannberg A and McGreevy R L 2000 *Phys. Rev.* B **61** 487
[29] Jóvári P and Pusztai L 2001 *Phys. Rev.* B **64** 14205
[30] Keen D A and McGreevy R L 1990 *Nature* **344** 423
[31] Wang Y, Lu K and Li C 1997 *Phys. Rev. Lett.* **79** 3664
[32] Bionducci M, Navarra G, Bellissent R, Concas G and Congiu F 1999 *J. Non-Cryst. Solids* **250** 605
[33] Wicks J D and McGreevy R L 1995 *J. Non-Cryst. Solids* **192** 23
[34] DiCicco A, Taglienti M, Minicucci M and Filipponi A 2000 *Phys. Rev.* B **62** 12001
[35] de Lima J C, Raoux D, Tonnerre J M, Udron D, Machado K D, Grandi T A, Campos C E M and Morrison T I 2003 *Phys. Rev.* B **67** 94210
[36] Tengroth C, Swenson J, Isopo A and Borjesson L 2001 *Phys. Rev.* B **64** 4207
[37] Iparraguirre E W, Sietsma J and Thijsse B J 1993 *J. Non-Cryst. Solids* **156–158** 969
[38] Ohkubo T, Kai H and Hirotsu Y 2001 *Mater. Sci. Eng.* A **304–306** 300
[39] Pusztai L and Sváb E 1993 *J. Phys.: Condens. Matter* **5** 8815
[40] Poulsen H F, Neuefeind J, Neumann H-B, Schneider J R and Zeidler M D 1995 *J. Non-Cryst. Solids* **188** 63
[41] Ressler T 1997 *J. Physique Coll.* **7** C2
[42] Stern E A, Sayers D E and Lytle F W 1975 *Phys. Rev.* B **11** 4836
[43] Rehr J J 1991 *J. Am. Chem. Soc.* **113** 5135
[44] Tani Y, Shirakawa Y, Shimosaka A and Hidaka J 2001 *J. Non-Cryst. Solids* **293–295** 779
[45] de Lima J C, Trichês D M, Grandi T A and de Biasi R S 2002 *J. Non-Cryst. Solids* **304** 174
[46] Lague S B, Barnes A C, Archer A D and Howells W S 1996 *J. Non-Cryst. Solids* **205–207** 89
[47] Holender J M and Gillan M J 1996 *Phys. Rev.* B **53** 4399
[48] Holender J M and Gillan M J 1996 *J. Non-Cryst. Solids* **205–207** 866
[49] Choi J, Gurman S J and Davis E A 2002 *J. Non-Cryst. Solids* **297** 156
[50] Waseda Y 1980 *The Structure of Non-Crystalline Materials (Liquid and Amorphous Solids)* (New York: McGraw-Hill)
[51] Kugler S, Pusztai L, Rosta L, Chieux P and Bellissent R 1993 *Phys. Rev.* B **48** 7685